JOURNAL OF PROPULSION AND POWER
Vol. 23, No. 5, September–October 2007

Evolution of Carbonaceous Aerosol and Aerosol Precursor Emissions Through a Jet Engine

K. D. Brundish,* A. R. Clague,† and C. W. Wilson‡
QinetiQ, Farnborough, Hampshire, GU14 0LX England, United Kingdom
R. C. Miake-Lye,§ R. C. Brown,¶ and J. Wormhoudt**
Aerodyne Research, Inc., Billerica, Massachusetts 01821
S. P. Lukachko,†† A. T. Chobot,‡‡ C. K. Yam,§§ and I. A. Waitz¶¶
Massachusetts Institute of Technology, Cambridge, Massachusetts 02139
and
D. E. Hagen,*** O. Schmid,††† and P. D. Whitefield‡‡‡
University of Missouri–Rolla, Rolla, Missouri 65409

DOI: 10.2514/1.27502

This study conducted during the summers of 2000 and 2001 represents the first measurement and model intercomparison that tracks detailed gaseous and aerosol emissions through a gas turbine engine. Its primary objective was to determine the impacts of engine operational state on the evolution of carbonaceous aerosol and aerosol precursors. Emissions measurements were performed at the exit of a combustor and at the exit of a full engine for a gas turbine engine typical of the in-service, commercial aircraft fleet. Measurements were compared to model simulations of changes in gaseous chemistry. As predicted by the model simulations, results show no significant modifications to the aerosol distribution along the postcombustor flowpath. The oxidation of NO to HONO was measured. Trends with engine power setting and sulfur loading were at the level of estimated uncertainty limits. Simulations of the fluid and chemical processes through the turbine and exhaust nozzle correctly captured HONO trends and matched experimental data within measurement uncertainty. This suggests that the employed modeling approach is valid for HONO chemistry, and more generally, because HONO results from NO oxidation via the hydroxyl radical, indicates the importance of OH-driven oxidation through the engine. These results indicate that the chemical and physical processes occurring in the turbine are important in determining aircraft engine emissions.

Received 25 August 2006; revision received 24 April 2007; accepted for publication 25 April 2007.

*Propulsion Engineer, Fuels and Lubricants Center, Cody Technology Park, Ively Road; KDBRUNDISH@qinetiq.com.

†Capability Leader, Fuels, Fuels and Lubricants Centre, Cody Technology Park, Ively Road; arclague@qinetiq.com.

‡Professor, Department of Mechanical Engineering, University of Sheffield, MD56, Mappin Building, Mappin Street, Sheffield, UK S1 3JD; c.w.wilson@sheffield.ac.uk.

§Principal Scientist and Director, Aero-Thermodynamics, 45 Manning Road.; rick@aerodyne.com.

¶Scientist, Applied Physics Laboratory, The Johns Hopkins University, MS MP3-W110, 11100 Johns Hopkins Road, Laurel, MD 20723; Robert.Brown@jhuapl.edu.

**Principal Scientist, 45 Manning Road; jody@aerodyne.com.

††Post-Doctoral Fellow, Department of Aeronautics and Astronautics, 77 Massachusetts Avenue; sluka@mit.edu.

‡‡Post-Doctoral Fellow, Department of Aeronautics and Astronautics, 77 Massachusetts Avenue.

§§Post-Doctoral Fellow, Department of Aeronautics and Astronautics, 77 Massachusetts Avenue.

¶¶Professor of Aeronautics and Astronautics, Director of the Partnership for AiR Transportation Noise and Emissions Reduction (PARTNER), 33-408, 77 Massachusetts Avenue; iaw@mit.edu. Fellow AIAA.

***Professor of Physics, Director of the Cloud and Aerosol Sciences Laboratory (CASL), G-7 Norwood Hall; hagen@umr.edu.

†††Senior Scientist, GSF National Research Center for Environment and Health, Institute for Inhalation Biology, Ingolstaedter Landstrasse 1, D-85764 Munich/Neuherberg, Germany; otmar.schmid@gsf.de.

‡‡‡Professor and Chair of Chemistry, Director of the Center of Excellence for Aerospace Particulate Emissions Reduction Research, G-11 Norwood Hall; pwhite@umr.edu. Member AIAA.

Nomenclature

d_g	=	geometric mean diameter
$EI(M)$	=	mass based emission index
$EI(N)$	=	number based emission index
$EI(SA)$	=	surface area based emission index
M	=	mass
N	=	size distribution in terms of number
V	=	volume
σ_g	=	geometric standard deviation

I. Introduction

AVIATION-RELATED sulfate, carbonaceous aerosols (soot), and their precursors have been implicated in a number of physical and chemical processes in the upper atmosphere. The particle emissions from aircraft engines during flight contribute directly to the background aerosol loading. In addition to direct radiative effects, aerosol emissions from aircraft engines contribute to contrail formation, could play a role in ozone depletion (IPCC report, Chapter 2 [1]), and have an undetermined but possibly important effect on clouds. The latter consequence is of particular interest to this study. Cirrus cloud formation can increase by up to 25% within flight corridors [1] and contribute significantly to the greenhouse effect. However, much is still unknown about aviation effects on cloud formation. In the case of the potential impact of aerosol emissions, progress to date has been limited by the paucity of experimental data through which to verify the mechanisms of aerosol formation. This study addresses the need to characterize the amount and nature of aircraft aerosol emissions so that their potential environmental impacts can be better understood.

The present study addresses this scarcity of data, providing the first consistent set of measurements for aerosol and aerosol precursor species obtained at both the combustor and the engine exit of a gas turbine engine typical of the in-service, commercial fleet operating at realistic cruise conditions. The analysis presented here is based on

the data collected in the 2000 and 2001 campaigns and reported in the NASA technical report (NASA/CR-2002-211900). Its primary objective was to determine impacts of the engine operational state on the evolution of carbonaceous aerosol and the aerosol precursors SO_2, SO_3, and HONO. Aerosol precursor species evolve due to postcombustor oxidative processes driven by O and OH. Thus, SO_3 and HONO are particularly good indicators of the degree of oxidation occurring in the turbine and exhaust nozzle and are the focus of the measurements in this study. SO_3 is of added interest due to its role as an intermediate in forming H_2SO_4, which has been implicated in the formation of additional volatile sulfate aerosol after the exhaust has left the engine. Because SO_2 and NO are the source gases for SO_3 and HONO produced in the turbine, their measurement is important for complete quantification of SO_x and NO_y [2,3]. SO_x consists of SO_2 and its oxidation products, especially SO_3 and H_2SO_4 in aircraft exhaust. Reactive nitrogen (NO_y) consists of NO_x and its oxidation products, the most important of which are NO, NO_2, HONO, and HNO_3, as well as aerosol NO_3, peroxyacetyl nitrate (PAN), and other organic nitrates, NO_3, N_2O_5, and HNO_4, some of which may only become important long after emission in the atmosphere. Carbonaceous aerosols form in the primary zone of the combustor and may evolve through gas-to-particle processing and coagulation as well as burnout as they proceed to the engine exit. Hydrocarbon aerosol precursor gases were not addressed in this study.

II. Experimental Setup and Test Schedule

The entire study was conducted at QinetiQ facilities in Farnborough, U.K., using equipment dedicated to aircraft engine and combustor tests. These facilities are instrumented with a number of independent controls allowing more extensive manipulation of engine parameters, such as air bleeds and inlet blade angles, than available during normal on-wing operation. Diagnostic facilities were set up and operated by research teams from QinetiQ, Aerodyne Research, Inc., (ARI) and the University of Missouri–Rolla (UMR). The study was divided into two phases each of approximately one month's duration. The first phase occurred in August/September 2000 and focused on the combustor exit plane measurements. The second phase took place in July 2001 and involved an identical set of measurements at the engine exit. This section describes the experimental setup and test conduct.

A. Sampling

Studies of aerosols and their precursors in an engine environment require extractive sampling. As a result of widely different physical parameters at the engine and combustor exits, source-specific probes were employed.

1. *Combustor Probes*

The combustor probe developed for this study was required to supply measurement systems for standard gas analysis (SGA), aerosols (AE), and aerosol precursors (AP). Sufficient flow to the three systems [10 l/ min gas analysis and 14 l/ min Society of Automotive Engineers (SAE) smoke for SGA, 1.4 l/ min for AE, 1–2 l/ min for AP] was desirable so that measurements could be performed simultaneously. Further requirements included the minimization of surface contact with the sample flow, which can perturb the reactive gas, and minimization of thermophoretic deposition of aerosol particles onto cold probe surfaces.

The internal diameter (ID) of the probe is larger (39.3 cm length, 0.8 cm ID) than normally employed for gas extraction to reduce the surface area/volume ratio. This short, large diameter operates at the combustor pressure and is followed by a splitter block in which the sampled gas is divided into three streams to supply the SGA, AE, and AP measurement systems. The small orifice at the entry to the AP feed allows subatmospheric pressures (necessary for the AP measurement equipment) to be achieved. Downstream of this small orifice, nitrogen is injected along the wall to further minimize contact between the combustion gas and the probe wall. The AE and SGA feeds are taken at an angle of approximately 45 deg to reduce flow disturbance. Just downstream of the AE feed, particle free dilution air is added to reduce coagulation and condensation effects on the measured aerosols.

Exit gas temperatures of up to 2000 K can be found at the combustor exit, and as a result, the probe must be water cooled to maintain life. Cooling is also required to reduce the gas sample temperature sufficiently to quench reactions such that almost all sampled species arriving at the measurement systems are representative of those in the exit plane. This is particularly important in halting the chemistry of CO and NO_x, and for this purpose, the sample must be quenched to 150 ± 5°C. The sample temperature cannot be lowered further without risk of unburned hydrocarbon and water condensation. Such condensation can remove oxides of nitrogen and sulfur, by conversion to nitric and sulfuric acid, and can change aerosol particle size distributions.

During testing, heat stress warped the specialist combustor probe. Although this did not restrict the use of the data obtained through the probe, it did introduce an uncertainty in determining its position at the combustor exit. Thus, the acquired data are used to examine relationships among species without spatial resolution. A standard probe, typically used in the combustor test facility, was employed in a subsequent test to obtain a spatially resolved reference database.

2. *Engine Probes*

Two probes were required for engine exit measurements. One probe supplied the SGA and AE measurement systems with samples from a number of points on a diametrical traverse across the engine exhaust. The second probe was designed to supply the AP system and was fixed in position to allow aerosol precursor measurements.

The SGA/AE probe consists of a stainless steel sampling tube within a water cooled jacket. As with the specialist combustor probe, cooling water was supplied to ensure probe life and to condition the sample to 150 ± 5°C. To guarantee the fidelity of the sample for smoke and all other aerosols, and to allow the probe to move, the sample line is coiled and unwinds with horizontal motion of the probe. Although the coil adds line length, it guarantees that the bend radii are always smoke and aerosol compliant (i.e., greater than 10 times sample line diameter). Although it was possible to add dilution air at the sample tip of the traversing probe, dilution air was added at 0.5 m downstream to be consistent with the combustor studies. The initial 0.5 m of the sample line was, however, temperature controlled to ensure condensation did not occur.

The AP probe consisted of a length of 12.7 mm ID silica-coated stainless steel tubing inside a support and water-jacket assembly, followed by a second length of uncooled coated stainless steel tubing of 15.88 mm outer diameter (OD). The probe terminates in a sampling cone with a 0.79 mm orifice and a 20 deg internal expansion full angle. This orifice resulted in a pressure drop from the exhaust to 16–18 torr in the multipass cell component of the AP measurement system. Shortly after the probe tip, the sample line turns through 90 deg to the AP tunable diode laser (TDL) instrument, which was placed just outside the exhaust stream.

To avoid collision with the traversing SGA/AE probe, the AP probe was offset from the engine centerline. Previous testing of the engine showed a near uniform distribution of emissions and temperature within a 50 mm radius of the center. This position also coincided with peak values of temperature and emission concentrations. The AP probe was therefore radially offset 50 mm. Both probes were located 460 mm downstream from the engine exit plane. This distance allowed adequate separation of the probes from the engine to avoid interaction (e.g., blockage effects), but was within the engine diameter (0.5 m) distance specified by the International Civil Aviation Organization (ICAO) regulations of measurement technique [4].

B. Measurement

The combustor operated in the stand alone test was the same as that used in the full-engine tests. However, for combustor exit measurements, only one of the 10 can-annular units installed in the

engine was mounted for sampling. Combustor and engine exit emissions measurements of CO, CO_2, NO, NO_2, O_2, and SAE smoke using the SGA system were performed in accordance with SAE Aerospace Recommended Practices (ARP) 1256 Rev B, 1179 Rev B, and 15333 [5–7]. Note that the combustor operates in compliance with current ICAO emissions standards for aircraft NO_x, CO, HC, and smoke. All concentrations included within this paper are corrected for inlet air humidity, cross interference effects, and dried sampling. Postprocessing also includes calculations of combustor air–fuel ratio (AFR), combustion efficiency, and gas temperature. Sections II.B.1 and II.B.2, respectively, examine the AP system for measurement of gaseous aerosol precursors and the AE system for carbonaceous aerosol measurement.

1. Aerosol Precursors

The main component of the AP measurement system is an infrared TDL apparatus [8,9]. A 15 cfm (cubic feet per minute) mechanical vacuum pump was used to draw the exhaust sample through a multipass cell. A diaphragm pump withdrew a small fraction of this flow, just downstream of the multipass cell, and passed it through a nondispersive infrared CO_2 measuring device (Vaisala GMT221). Ratios of trace gas to CO_2 concentrations were used to compute emission indices.

The apparatus used in the combustor test differed from that used for the engine in two ways. First, a different probe was used to sample the species at the combustor exit. As mentioned previously, after dividing the probe flow for the three measurement systems, the TDL sample passed through a small (0.03 cm diam) orifice of finite length (0.1 cm). This orifice resulted in a pressure drop from the 7–8 atm (5000–6000 torr) combustor pressures to the 25–35 torr multipass cell pressures. A detailed description of the TDL sample extraction system is reported elsewhere [10]. The second difference was that the CO_2 measuring device was not installed during the combustor tests. To measure a major species concentration related to the fuel flowrate, we relied on the fact that each spectral region also contained absorption lines of water vapor. However, this requires the subtraction of the exhaust water level due to humidity in the inlet air, and that in turn requires an accurate knowledge of the dilution factors. To determine the dilution factor for each set nitrogen flow, averages were made of TDL water measurements (on diluted flow) and CO_2 measurements made with the SGA system (on undiluted flow). Ratios of trace gas to individual H_2O concentrations (corrected for inlet air humidity measured with the SGA system, using the dilution factors) were used to compute emission indices.

The TDL apparatus used two lasers, one devoted to measuring HONO in the spectral range 1666–1667 cm^{-1} and one for sulfur oxide species (SO_2 at 1382–1383 cm^{-1} and SO_3 at 1401–1402 cm^{-1}). The SO_2 measurement has the constraint that its fraction in the exhaust has an upper limit defined by the fraction of sulfur in the fuel. Within the estimated uncertainty limits for TDL measurements and fuel analyses, the SO_2 measurements did not measure more than the total fuel sulfur. The uncertainty limits mean that other sulfur species could still be up to 20% of the total sulfur, and thus must be measured directly rather than by difference. Laboratory observations of SO_3 produced an accurate high resolution spectral model, and detection limits for SO_3 in the multipass cell as low as 15 ppbv (parts per billion by volume) were achieved during the tests, corresponding to an SO_3 fraction of total sulfur species of 0.001. No SO_3 was observed in either combustor or engine tests, and our laboratory experiments suggest this was due to losses in the sampling system with water vapor present. Therefore, the actual SO_3 fraction in the exhaust could be much larger than 0.001 and was not determined by our observations.

2. Aerosols

A description of the instrumentation and general measurement methodology and a discussion of measurement uncertainties can be found in [11]. Source emissions were extractively sampled from the exit plane of the combustor at elevated pressure (7–8 bar) using the specialist probe. The sample was immediately diluted with particle free dry air at 150°C to inhibit any condensation and coagulation in the sampling line and to reduce the concentration of carbonaceous aerosol arriving at the diagnostic facility. The optimum dilution was found by gradually increasing the dilution flow to the point, where further addition of diluent produced the same relative responses in total particle and CO_2 concentrations as well as in the vapor pressure of H_2O. Typical dilution ratios ranged from 7:1 to 10:1. The water content in the sample line was continuously monitored using a dew point hygrometer. Once diluted, but still at elevated pressure, the total aerosol concentration and size distribution for particle diameters >800 nm were measured close to the sampling probe (<3 m) in real time with a laser particle counter (LPC). After passing through the LPC the sample underwent a controlled depressurization in a pressure reduction facility to 1 bar for further analysis. The pressure reduction facility [11] consists of a series of eight calibrated orifices designed to cause adiabatic, subsonic expansions of the sample air without generating supersaturated conditions, which could lead to gas-to-particle conversion and hence alter the particle size distribution. It is housed in an oven operated at 150°C. Laboratory experiments were performed with pressurized particle free, moist air to verify that gas-to-particle conversion does not occur during the expansions. In addition, particle loss was determined experimentally and is included in the data reduction algorithm. Care was taken to ensure that there were no sharp bends in the path to the LPC to avoid impaction losses in the large particle regime. Once diluted and depressurized, the sample was conducted at a flow rate of about 10 l/ min through 22.6 m of line (4.3 m stainless steel tubing of 4.65 mm ID followed by 18.3 m high penetration flexible hosing of 6.4 mm ID) to the aerosol diagnostic facility. The penetration coefficients for the sampling trains were determined experimentally [11] using monodisperse, neutralized aerosols for the operating conditions experienced during testing. This was done for the sampling trains leading to the condensation nucleus counter used for total particle concentration and the differential mobility analyzer used for size distribution work. Size dependent penetration functions were determined and used in the data reduction analysis.

Engine exit samples were extracted using the traversing probe (see Sec. II.A.2). This sample was also immediately diluted with particle free dry air at 150°C with typical dilution ratios ranging from 7:1 to 10:1. The diluent air was introduced to the sample stream through a port in the sample line located 0.5 m downstream of the sampling probe orifice, a similar distance to that of the diluent introduction point for the combustor measurements. Once diluted, the sample was conducted to the aerosol diagnostic facility through sample lines similar to those used in the combustor measurements.

C. Test Conduct

Engine testing was performed on a QinetiQ research engine of a generic type typical of many currently flying, but of lower pressure and bypass ratios than modern production engines. It is a can-annular aeroengine and for the combustor tests, one of this engine's 10 combustors was separately mounted in the QinetiQ combustor test rig. The combustion system used in both sets of tests is compliant with the Committee on Aviation Environmental Protection (CAEP) 4 emissions standards. The cruise condition used in the tests directly compares to that of legacy engines still in use, while an uprated cruise condition was employed to reflect more accurately the cruise condition of modern production engines. The limit to this uprated condition was the pressure capability of the test facility.

Although not fully representative of the annular combustors typical in modern engines, more experimental control is afforded by the can-annular system used in these tests. Separate control of temperature (up to 900 K, nonvitiated), mass flow (up to 5 kg/s), and pressure (up to 10 bar) were available, allowing a wide variation of combustor inlet conditions to be achieved. The primary condition of interest for this study was cruise. Modeling simulations of aerosol precursor chemistry performed before the test suggested it would be prudent to conduct measurements at higher temperatures than normally achieved at cruise for the test engine to maximize the chances for measurement of change in aerosol precursor species.

Table 1 Test operating conditions

	Cruise	Uprated cruise
Temperature, K	566	588
Pressure, bar	7.1	8.0
Mass flow, kg/s	2.1	2.3
Air: fuel ratio	66	56

Testing at higher operating temperatures is also more representative of modern civil gas turbine cycles. A thermodynamic cycle model of the engine was used to determine the maximum combustor exit temperature that could be achieved while limiting the combustor inlet pressure to 10 bar, the upper limit of the combustor test facility. By adjusting the compressor inlet guide vanes and engine bleeds, the maximum combustor exit temperature achievable without engine stall or surge was derived. This is termed uprated cruise in the following sections. The nominal operating conditions used in the tests are given in Table 1.

One objective of the measurement program was to examine several fuel sulfur contents. Two sulfur levels representing low and typical levels found in aviation fuel and a high concentration to exaggerate any effect of sulfur content on emissions were sought in the test program. Fuel sulfur levels achieved for operating conditions are shown in Table 2.

For the engine test, target sulfur levels were based upon those where maximum data were available from the combustor test program. Achieved sulfur levels were <10 ppmm (low), 460 ppmm (medium), and 2060 ppmm (high). The same sulfur additive, dimethyl disulfide (DMDS), and low-sulfur fuel were used in the combustor and engine tests. Many low-sulfur fuels are hydrotreated and the aromatic content is reduced to insignificant amounts (<0.5%) which affects aerosol emissions. A fuel with an aromatic content of 15%, typical of current aviation fuels, was selected to avoid influences on soot emissions. It should be noted that the sulfur doping technique varied between the combustor and engine tests. For combustor measurements, the sulfur additive was pumped into the fuel system about 2 m upstream of the fuel injector, which allowed adequate mixing before injection into the combustor. Although the doping pump was calibrated, its delivery rate could fluctuate and points with sulfur values significantly outside the stated levels were recorded. Sulfur levels were confirmed by a separate fuel analysis as listed in Table 2. Because the use of a doping pump had resulted in fluctuations in the fuel sulfur level, the sulfur dopant was mixed with the bulk fuel before the run for engine tests.

A series of measurement sessions with at least three fuel sulfur levels was performed. Identical schedules were used for each test. After an initial thermal adjustment period of approximately 15 min at idle condition, power was increased to the uprated cruise condition. The combustor or engine was run at uprated cruise for approximately 2 h, after which the power was reduced to cruise. The combustor or engine was then run for a further 2 h at cruise condition before returning to idle for a further 15 min. During the 2 h period on condition (both cruise and uprated cruise), trace species measurements were taken. For the engine test, instrumentation was logged and subsequently used in conjunction with the engine model to derive the achieved running conditions.

III. Results

Particle measurements indicated no significant modifications to the carbonaceous aerosol distribution along the postcombustor gas path. This suggests that the formation of the carbonaceous particles with a typical modal diameter of about 40 nm is completed at the combustor exit plane. At the combustor and to a lesser degree at the engine exit we observed the appearance of nucleation mode particles ($d < 20$ nm) that most likely originated from gas-to-particle conversion of noncarbonaceous components [12,13].

SO_2 and HONO concentrations were measured and attempts were made to measure SO_3. The clearest trend in HONO observations was a substantial increase through the postcombustor gas path. Trends with engine power setting and sulfur loading were at the level of estimated uncertainty limits. Simulations of the fluid and chemical processes through the turbine and exhaust nozzle correctly captured HONO trends and matched experimental data within measurement uncertainty. This suggests the importance of OH-driven oxidation through the engine since the modeled HONO evolution results from NO oxidation via the hydroxyl radical.

Sections III.A and III.B review and analyze measurement results obtained from the SGA, AE, and AP instrument systems, respectively. Comparison of these results provides a basis on which to evaluate the evolution of gaseous and carbonaceous aerosol precursors and carbonaceous aerosols through the postcombustor gas path. Section III.D presents model simulations of these processes that are used to further reflect on the measurements obtained.

A. Standard Gas Analysis

Measurements of exit plane CO, NO_x, NO, NO_2, CO_2, O_2, and SAE smoke number emissions were performed for a range of different fuel sulfur contents using the SGA instrument system [10]. Tests using the same configuration showed little variation and indicated that the species measured by the standard gas analysis were not affected by sulfur concentration.

1. SGA Combustor Results

Data were collected using both the specialist and standard combustor probes. Comparison of the samples taken with the two probes indicated that CO emissions were affected by internal reactions within the specialist probe. Internal probe reactivity was modeled for the standard species using a chemical kinetics package to determine a correction factor. Density-averaged values from both the standard and specialist probe for the uprated cruise low-sulfur condition matched to within 6%. Averaged data for other conditions could not be obtained because of the lack of accurate spatial reference.

Data from both probes were used to evaluate the effects of the sulfur concentration and power setting on emissions. It was found that fuel sulfur level had no discernible effect on emissions of CO_2, NO_x, CO, or smoke number. Measured concentrations of these species were consistent with the power setting, with emissions of CO_2 and NO_x being higher for uprated cruise, reflecting the richer (and hotter) combustor operation. However, these differences were small, suggesting that the differences between the standard and the uprated cruise conditions themselves were not large.

2. SGA Engine Results

Measurements performed across the engine centerline show peaked profiles for all emissions, with a concentration maximum at the center point. The plume edge was determined to be between 260 and 265 mm radius, beyond which dilution from entrained air dominated the measurements. CO_2 concentration at the center point was used as a daily check to ensure consistent emissions results were obtained. Good repeatability was achieved for the center point, but it was found that the low-sulfur CO_2 values were lower for other points.

Table 2 Fuel sulfur levels achieved for operating conditions

Emission source	Operating condition	Fuel sulfur concentrations, ppmm
Combustor	Uprated cruise	8, 550, 1600, 2350, 2500, and 11,650
	Cruise	8, 830, and 2300
Engine	Uprated cruise	<10, 460, and 2060
	Cruise	<10, 460, and 2060

This suggests that the low-sulfur tests were performed with the combustor operating more fuel lean (and thus cooler) than for the medium and high sulfur tests. Engine instrumentation confirmed this conclusion, but the cause for the difference was not identified. Engine model and instrumentation data also showed that the combustor AFR was progressively more fuel rich (lower AFR) for each run day. Although the difference in AFR between medium and high sulfur running days was small, too small to be seen in CO_2 concentration changes, this may have affected NO_x as it is more sensitive to gas temperature.

Emissions measurements were consistent with previously measured data for the same engine. All emissions were higher for uprated cruise compared to the cruise condition. Lower HC and CO concentrations measured for cruise suggested slightly higher efficiencies than for uprated cruise, although the variation in HC was within the experimental error associated with the gas analyzer. CO_2 increases corresponded with the richer operation of the combustor for uprated cruise. NO_x increases were also expected, although the change in combustion temperature (on which they are partly dependent) with uprated cruise was small and thus differences were minimal.

It was found that the fuel sulfur level had no discernible effect on emissions of CO_2, CO, HC, or overall smoke number for a given power setting. Variations in the smoke number were within the measurement accuracy and therefore no trend could be established. It was noted that for the uprated cruise, low-sulfur condition, both CO and HC were higher than for other conditions, resulting in a lower efficiency. NO_2 concentrations were noticeably lower for this condition, but probe effects cannot be discounted. NO_x values increased with increasing sulfur levels, although this may also be due to day-to-day variation.

3. *Comparison of SGA Combustor and Engine Results*

To ensure that modeling simulations could use combustor exit data as boundary conditions and engine exit data for validation, it was important to compare the operation of the combustor in both test programs. The engine tests were designed so that the conditions within the combustors of the engine were as close to those in the combustor tests as possible. With the exception of one test, the agreement between the operating conditions of the combustor and engine tests agreed to within 5% for inlet temperature and AFR. Pressure was more difficult to control and varied by up to 20%. The one exception to this agreement was the low-sulfur uprated cruise engine test, which showed differences in all parameters of up to 20%.

A comparison of measurements at the engine exit, corrected for bypass dilution, against combustor exit measurements was performed to determine the effects of these differences. The dilution factor varied slightly depending on the operating condition. Although the bypass ratio of the engine is approximately 0.62, the dilution factor is higher as some of the core air bypasses the combustor and is used for downstream cooling. The dilution factor was calculated using the engine model baselined against engine instrumentation measurements performed during the tests. The calculated dilution ratio from the combustor exit to the engine exit plane was 2.1 ± 0.05 for all power conditions.

Table 3 shows a comparison of the average emissions data for the uprated cruise, medium sulfur condition. The engine data have been averaged and multiplied by the dilution factor. Note that a full combustor exit traverse was not achieved and thus air cooling close to the combustor wall was missed. This has the effect of biasing the averaged results to be more fuel rich, as shown with the AFR averages. Other emissions, such as CO_2 and NO_x, will also be different as a result. For the condition of Table 3, the target AFR of 55 was achieved. The main reason for CO_2 concentration differences between combustor and engine exit emissions is traverse coverage, as with AFR. Combustor exit NO_x emissions should remain constant between the combustor and engine exits, as the temperatures through the hot section are insufficient to create further thermal NO_x. Although combustor levels are not identical to the engine concentrations, the AFR differences suggest comparability. Again, incomplete traverse would account for the higher measured combustor levels. Unburned hydrocarbon levels match to within 4 ppmv, which is within the experimental uncertainty of the gas analyzer. Measurement error on the small levels of NO_2 is in the region of $\pm 30\%$. However, even when accounting for this error and differences due to incomplete traverse, NO_2 levels appear to increase from combustor exit to engine exit, a trend suggested by previous and current modeling efforts as NO oxidizes to NO_2. Emission index (EI) values are also included in the average tables. Although EI values are nondimensional, being ratios of trace species mass to mass of fuel, incomplete traverse would have the same effect on EI as all of the fuel may be accounted for but not all of the air. Thus, the averaging process would still bias EI values to be more fuel rich. In general, even though combustor inlet pressures were different during the two tests, concentration levels for measured species are expected to remain kinetically stagnant between the combustor and engine exits [e.g., CO_2, NO_x, and unburned hydrocarbons (UHC)] compare well. It can be said with reasonable confidence therefore, that the inlet and outlet conditions for the combustor during the combustor and engine test were well matched allowing comparison between the two data sets.

B. Aerosol Precursors

Aerosol precursor data are summarized in Table 4. Entries are distinguished by the parameters of fuel sulfur loading and power level. However, neither the power level nor the sulfur doping technique was precisely constant between the combustor and engine tests, as has already been described. The TDL sampling orifice plugged during the combustor test day using undoped, low-sulfur fuel, so the two data sets listed are medium and high levels of fuel sulfur. In the engine test, signal-to-noise problems made the analysis of the high sulfur data set more difficult than for the medium sulfur data, hence the larger error bars. The same problems, caused by

Table 3 Comparison of combustor and engine exit SGA measurements for uprated cruise, medium sulfur condition

	Engine	Combustor
CO_2 %	3.73	4.09
H_2O %	6.58	5.36
CO ppmv	70	94
HC ppmvC	6	2
NO_2 ppmv	7	4
NO ppmv	57	94
NO_x ppmv	64	98
Combustion efficiency %	99.89	99.89
AFR	57	49
EICO, g/kg	3.8	4.7
EIHC, g/kg	0.2	4.7
EINO, g/kg	5.1	7.6
$EINO_x$, g/kg	5.8	7.9

Table 4 HONO sampling observations

	Medium sulfur	High sulfur
Combustor tests		
Fuel sulfur levels, ppmm	400–830	1600–2350
HONO exhaust gas concentrations (standard deviations)		
HONO ppbv (cruise)	300 ± 60	300 ± 80
HONO ppbv (uprated cruise)	385 ± 90	300 ± 100
HONO emission indices (standard deviations)		
HONO EI (cruise)	0.025 ± 0.0045	0.032 ± 0.007
HONO EI (uprated cruise)	0.031 ± 0.0055	0.021 ± 0.0055
$EI(HONO)/EI(NO_x)$, *% (estimated total error limits)*		
$HONO/NO_x$ (cruise)	0.45 ± 0.14%	0.46 ± 0.14%
$HONO/NO_x$ (uprated cruise)	0.32 ± 0.09%	0.26 ± 0.11%
Engine tests		
Fuel sulfur levels, ppmm	<10	2060
HONO exhaust gas concentrations (standard deviations)		
HONO ppbv (cruise)	674 ± 16	500 ± 100
HONO ppbv (uprated cruise)	713 ± 21	600 ± 130
HONO ppbv (idle)	180 ± 50	——
HONO emission indices (estimated total error limits)		
HONO EI (cruise)	0.108 ± 0.023	0.076 ± 0.021
HONO EI (uprated cruise)	0.102 ± 0.021	0.081 ± 0.024
HONO EI (idle)	0.03 ± 0.01	——
$EI(HONO)/EI(NOx)$, *% (estimated total error limits)*		
$HONO/NO_x$ (cruise)	2.0 ± 0.5%	1.1 ± 0.4%
$HONO/NO_x$ (uprated cruise)	1.9 ± 0.4%	1.3 ± 0.4%
$HONO/NO_x$ (idle)	1.0 ± 0.5%	——

etalon fringes in the infrared spectra, were worse for a medium sulfur data set, which is not reported here.

There are two types of error limits indicated in Table 4, depending on the comparisons to be made using the data. For evidence as to whether a change in HONO concentration with power setting is significant, when that change occurs in the middle of a test day with all other parameters remaining constant, the appropriate error limit is an estimate of random errors (precision). For this the standard deviation in repeated observations is used. If we want to compare observations made on different days, or to compare observations with model predictions, an estimate must be added of possible systematic errors. These accuracy error limits are estimated [14] from a series of systematic error sources, added in quadrature to the above precision error limits.

1. *Combustor Precursor Aerosol Results*

The 30 values of HONO concentration obtained during the combustor tests were divided into four sets of 5 to 10 each. In addition, each data point was obtained at a different spatial point in the combustor, over which there were some large variations in AFR. The mean of all 30 values of HONO EI was 0.026, with a standard deviation of 0.007 or a percentage variance (100*variance/mean) of 26%. By comparison, the average of the corresponding values of NO EI as reported in the standard gas analysis (before moisture corrections) was 7.1, and its variance was 10%. If we first ratio HONO EI to NO EI at each point, then average the ratios, that average value is 0.0038 or 0.38%. The variance in this set of ratios is 32% of the mean. If we ratio HONO to NO_x (the sum of NO and NO_2) the average of ratios is 0.0036 and the variance in the ratios is also 32% of the mean. These variance values are larger than the expected variance if the two EI arrays were uncorrelated, that is, the 28% variance obtained by adding 26% and 10% in quadrature. This means that there is no evidence for a significant correlation between NO or NO_x and HONO concentrations. The conclusion is that HONO is an approximately constant fraction of the NO or NO_x level even as that level varies.

The large standard deviations in the sets of HONO combustor exhaust concentrations, ranging from 20 to 33%, decrease slightly in the set of HONO EIs, whose fractional variances range from 17 to 26%. Because the array of combustor points sampled was different for each data set, differences between data subsets may not be due solely to a power setting effect, for example, but involve other systematic effects. We looked into the question of a systematic variation of HONO emission with position in the combustor, drawing on additional observations beyond those averaged in Table 4. One set of observations, of differences in HONO at five spatial points accessed over 30 min (more likely to bring out systematic trends than are averages over data points collected over several days), does show an increase in HONO moving from the wall to the center of the combustor. However, in general, we cannot say that the data set presented in Table 4 showed any systematic, steady-state differences in HONO concentration with position in the combustor.

The small fractions of HONO compared to NO and NO_x are expected [2,3]. These ratios also show no dependence on sulfur loading, and a decrease in going from cruise to uprated cruise power. Averaging over all high sulfur points gave a $HONO/NO_x$ ratio of 0.35 ± 0.14%, while averaging over all medium sulfur points gave 0.36 ± 0.10%. On the other hand, averaging over all cruise points gave 0.46 ± 0.09%, while averaging over all uprated cruise points gave 0.29 ± 0.07%. The above caveats regarding possible systematic effects notwithstanding, these average values are separated by more than their combined standard deviations. We conclude that there may have been a significant change in $HONO/NO_x$ with power setting, and that there was no observable effect of sulfur loading on HONO emission from the combustor. $HONO/NO_x$ ratios decreased in going from cruise to uprated cruise by an average factor of 1.6 for all data points, and similar factors applied for subsets of the full data set.

2. *Engine Aerosol Precursor Results*

In the engine exhaust data set, the small (6%) increase in the medium sulfur HONO concentration value in going from cruise to uprated cruise may still be significant because of the small random errors during this measurement period. A much larger difference is seen between cruise and idle. Although idle power was not a focus of this test, and the error limits on this observation are larger, it is clear that HONO emission is much lower at idle. We take these changes with power setting as evidence that HONO is sampled accurately by the probe, instead of being formed or destroyed in the probe to some

equilibrium level. When the conversion is made to EIs, the change between cruise and uprated cruise is reversed, with uprated cruise having a slightly lower HONO emission index. Idle is still clearly much lower. The much larger error limits for the high sulfur data sets mean it is difficult to be certain of any significant change with power setting, or even with sulfur loading.

The medium sulfur uprated cruise condition was leaner than planned, and this led to lower NO and NO_2 emission indices. In fact, uprated cruise NO and NO_2 emission indices are always lower than the corresponding cruise values, NO by 4 to 9% and NO_2 by at least 25%. Looking at the $HONO/NO_x$ entries in Table 4, it can be seen that this trend in NO_x does not reverse the EI change with power setting for medium sulfur, while it reinforces the result for high sulfur that uprated cruise HONO emission is larger than cruise. It is difficult to be certain whether either trend with power setting is significant. The comparison between medium and high sulfur values, in which systematic errors may play the most significant role, also should be summarized as not providing certain evidence of an effect on HONO emission with sulfur loading. The one clear qualitative difference is between HONO at flight power settings and at idle. Although standard gas analysis NO_x measurements were not made at idle periods used to measure HONO, a previously measured NO_x value was available and was used to compute the ratio in Table 4 (further increasing its estimated error).

The uncertainty limits for HONO concentration in Table 4 are estimates of precision only. They are, therefore, not the error limits which will be needed to compare with model predictions, which are total errors (accuracy limits) including both systematic and random errors. For medium sulfur, the error estimate comes almost entirely from the 20% systematic error limit, leading to a HONO value to compare with the model of 674 ± 140 ppbv. For high sulfur, adding 20% precision errors and 23% systematic errors in quadrature results in a total error of 30% and a HONO value for a model of 500 ± 150 ppbv.

3. *Comparison of Combustor and Engine AP Results*

In both combustor and engine tests, HONO variations with power may have been significant but are very close to the respective error limits, with the exception of the clearly lower levels at idle. The same uncertainty applies to the variation of engine exit HONO with fuel sulfur loading, while the combustor data set (containing a wide variation in ratios over the spatial points sampled) showed no change in average HONO/NO ratio with sulfur. The most certain trend in Table 4 is the increase in HONO emission going from combustor to engine exhaust. The HONO emission indices increase by factors of from 3 to 4 going from combustor to engine, while the $HONO/NO_x$ ratios for the most reliable engine data set, for medium sulfur fuel, are more than 5 times the average of all combustor values.

C. Aerosols

The main objective of the aerosol measurements was to determine carbonaceous aerosol concentration and size distribution in terms of number N, surface area SA, volume V, and mass M. For the conversion of the number size distribution into SA, V, and M, we assumed spherical particle shape and a particle density of 1.5 g/cm^3. Particle EIs were calculated based on aerosol concentrations and CO_2 levels [11]. Figures 1a and 1b depict the measured differential number and mass emission index, respectively, (diamonds) and bimodal curve fits (solid lines) measured at the combustor exit plane for uprated cruise power setting and medium fuel sulfur content. A rationale for the bimodal approach will be given later. The bimodal fit was performed simultaneously for all moments (N, SA, M), where each mode can be described by three characteristic parameters, namely, the total number EI [$EI(N)$], geometric mean (or count median) diameter (d_g) and geometric standard deviation (σ_g). No new fit parameters are introduced for the higher moments, because they can be calculated from $EI(N)$, d_g, and σ_g using the Hatch–Choate equations [15], i.e., the fitting procedure theoretically yields six independent parameters (2 modes with 3 parameters each) for each data set. To avoid convergence problems σ_g was assumed to be identical for both modes, i.e. $\sigma_{g,1} = \sigma_{g,2}$.

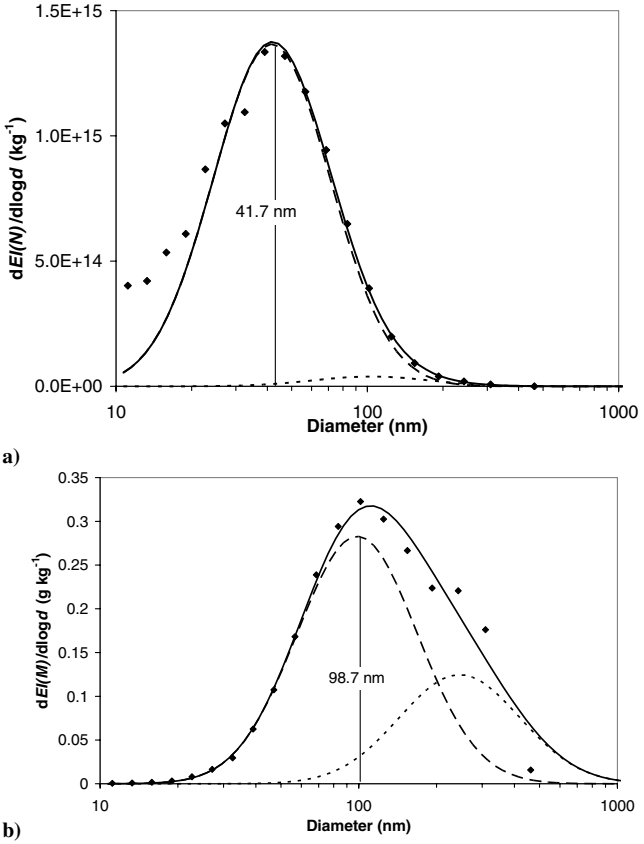

Fig. 1 a) Differential $EI(N)$ number distribution measured at combustor exit for uprated cruise power and medium fuel sulfur content. The diamonds represent the data, the solid line represents a bimodal lognormal curve fit, the long-dashed line represents the first mode, and the short-dashed line represents the second mode. b) Differential $EI(M)$ mass distribution measured at combustor exit for uprated cruise power and medium fuel sulfur content. The diamonds represent the data, the solid line represents a bimodal lognormal curve fit, the long-dashed line represents the first mode, and the short-dashed line represents the second mode.

The good quality of these fits can be seen from the solid black lines in Figs. 1a and 1b. For the combustor it is evident that the geometric mean diameter of the main (first) mode (long-dashed line) of $dEI(N)/d\log d$ and $dEI(M)/d\log d$ is at about 40 and 100 nm, respectively. The smaller (second) mode (short-dashed line) was at about 100 and 250 nm for $EI(N)$ and $EI(M)$, respectively. For the engine, the first mode was found to be relatively unchanged, but the second mode was more pronounced and shifted to larger sizes (150 and 315 nm) for $dEI(N)/d\log d$, respectively. Although the second mode contributes less than 4% to the overall $EI(N)$, it contributes about 30 and 50% to the measured $EI(M)$ of the combustor and engine, respectively. We believe that the second mode is an artifact due to nonisokinetic sampling [16], because both its magnitude and mean size correlated well with the relatively high ratio of the freestream velocity to sampling flow velocity (>120). To correct the data for nonisokinetic sampling artifacts we discarded the second (artifact) mode for the following analysis. It should also be noted that the sampling probe for the combustor work was a unique device. It had limited performance testing, and design constraints due to the specialized application inside a combustor may have induced probe effects that would also alter the particulate size distributions. In addition to the nonisokinetic sampling conditions, the constraint to introduce diluent downstream of the probe tip could have resulted in some size enhancement due to agglomeration, and high gas temperatures at the combustor exit may have produced large thermal gradients in the probe which could cause thermophoretic losses.

Table 5 Summary of combustor exit aerosol sampling observations

Fuel sulfur	Medium	Medium	High	High
SO_2 ppmm	830	550	2300	2350
Engine power	Cruise	Uprated Cruise	Cruise	Uprated Cruise
$EI(N)$, 10^{15} kg^{-1}	0.87 ± 0.17	0.80 ± 0.16	0.84 ± 0.17	0.90 ± 0.18
$d_{g,N}$, nm	42.1 ± 1.7	41.7 ± 1.7	48.4 ± 1.9	42.3 ± 1.7
σ_g[a]	1.713	1.709	1.696	1.726
$EI(SA)$[b], m^2 kg^{-1}	8.6 ± 2.2	7.7 ± 2.0	11.0 ± 2.9	10.1 ± 2.6
$d_{g,SA}$, nm	75.0 ± 6.0	74.0 ± 5.9	85.3 ± 6.8	76.8 ± 6.1
$EI(M)$[b,c] g $\cdot$ kg^{-1}	0.19 ± 0.06	0.17 ± 0.05	0.27 ± 0.08	0.23 ± 0.07
$d_{g,M}$, nm	100.2 ± 12.0	98.7 ± 11.8	112.8 ± 13.4	103.4 ± 12.4

[a]For lognormal distributions, the geometric standard deviation applies to all moments (here N, SA, and M).
[b]Spherically shaped particles were assumed.
[c]A particle density of 1.5 g $\cdot$ cm^{-3} was assumed.

Table 6 Summary of engine exit aerosol sampling observations

Fuel sulfur	Low	Low	Medium	Medium	High	High
SO_2 ppmm	8	8	460	460	2060	2060
Engine power	Cruise	Uprated cruise	Cruise	Uprated cruise	Cruise	Uprated cruise
$EI(N)$, 10^{15} kg^{-1}	0.77 ± 0.15	0.68 ± 0.14	1.5 ± 0.30	0.99 ± 0.20	1.5 ± 0.30	1.1 ± 0.22
$d_{g,N}$, nm	52.9 ± 2.1	52.2 ± 2.1	46.3 ± 1.9	46.3 ± 1.9	46.2 ± 1.9	46.0 ± 1.8
σ_g[a]	1.684	1.676	1.668	1.665	1.660	1.651
$EI(SA)$,[b] m^2 $\cdot$ kg^{-1}	11.7 ± 3.0	10.0 ± 2.6	17.1 ± 4.4	11.2 ± 2.9	14.9 ± 3.9	12.1 ± 3.1
$d_{g,SA}$, nm	91.0 ± 10.9	89.0 ± 7.1	78.2 ± 6.3	77.9 ± 6.2	77.3 ± 6.2	76.1 ± 6.1
$EI(M)$,[c] g $\cdot$ kg^{-1}	0.30 ± 0.09	0.26 ± 0.08	0.38 ± 0.12	0.25 ± 0.08	0.30 ± 0.09	0.26 ± 0.08
$d_{g,M}$, nm	119.4 ± 14.3	116.2 ± 14.0	101.6 ± 12.2	101.1 ± 12.1	100.0 ± 12.0	97.8 ± 11.7

[a]For lognormal distributions, the geometric standard deviation applies to all moments.
[b]Spherically shaped particles were assumed.
[c]Particle density of 1.5 g $\cdot$ cm^{-3} was assumed.

The pronounced deviation of measured and fitted $dEI(N)/d\log d$ for small diameters (<20 nm) (see Fig. 1a) indicates the presence of a third (nucleation) mode that probably originated from noncarbonaceous aerosol precursor components [12,13]. We made no attempt to include this mode in the curve fit, because the lower detection limit near 10 nm did not allow proper characterization of this mode. The data for the combustor and engine study are summarized in Tables 5 and 6, respectively, and are reported with the mean and estimated measurement uncertainty (1σ) for the various engine and fuel conditions [11]. The reported average aerosol parameters for the various fuel sulfur levels and engine power settings are based on weighted averages along the traverse. The error bars for $EI(N)$, $EI(SA)$, and $EI(M)$ represent the estimated accuracies [11] of 20, 26, and 31%.

While for the combustor, the aerosol (and CO_2) concentrations were relatively constant along the traverse (±20%), the probe position most distant from the engine center line (33 cm) sampled from the bypass air (90% bypass air, 10% sample). The peak aerosol concentration was 3.2 and 2.7×10^7 cm^{-3} for the combustor and engine, respectively.

1. *Combustor Aerosol Results*

The data indicate that there was no statistically significant dependence of the aerosol parameters on sulfur content or power setting. This is shown in Figs. 2 and 3 that depict the data for $EI(N)$ and $EI(M)$, respectively. The ratio of the cruise and uprated cruise data for $EI(N)$, $EI(SA)$, and $EI(M)$ (averaged over all sulfur levels) was 0.95, 1.10, and 1.08, respectively (see Table 5). This indicates that the EIs are invariant for the two power settings which is consistent with their operational similarity (see Table 1). The effect of fuel sulfur can be seen from the ratio of high and medium sulfur $EI(N)$, $EI(SA)$, and $EI(M)$ (averaged over power settings) that was 1.10, 1.29, and 1.43, respectively. Although this indicates a slight positive correlation between sulfur content and EIs, the trend is below or close to the estimated measurement uncertainties of 20, 26, and 31%, respectively.

Smoke number (SAE) correlations with aerosol number, surface area, and mass concentration were examined using all data points along a traverse (no averages). Almost no correlation was found with number ($R^2 = 0.13$), surface area ($R^2 = 0.18$), and mass concentration ($R^2 = 0.16$, slope = 0.13 mg/m^3/SAE, intercept= 2.9 mg/m^3), where the latter is depicted in Fig. 4 (triangles). All EIs correlated poorly ($R^2 < 0.11$) with air-to-fuel ratio.

2. *Engine Aerosol Results*

The aerosol data at the engine exit are summarized in Table 6. Again, the aerosol parameters show little dependence on fuel sulfur content and power setting (see Figs. 2 and 3). The ratio of cruise and uprated cruise $EI(N)$, $EI(SA)$, and $EI(M)$ (averaged over all sulfur levels) was 1.37, 1.31, and 1.29, respectively. Despite the slightly elevated particle emission for cruise conditions, the effect is close to the experimental uncertainties especially for $EI(SA)$ and $EI(M)$. For the ratio of high and medium sulfur $EI(N)$, $EI(SA)$, and $EI(M)$ (averaged over power settings), we found 1.05, 0.95, and 0.92, respectively, that constitutes no significant trend. On the other hand, dividing the average of high and medium by the low-sulfur data yields ratios of 1.75, 1.28, and 1.06 for $EI(N)$, $EI(SA)$, and $EI(M)$,

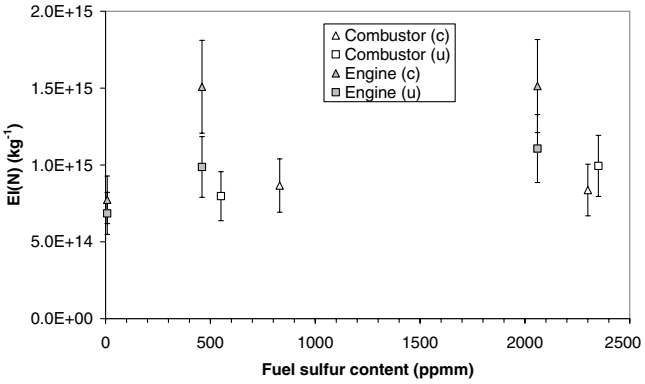

Fig. 2 Number emission indices $EI(N)$ for different sulfur levels, engine power settings (cruise *c*; uprated cruise *u*) and probe positions (combustor/engine exit).

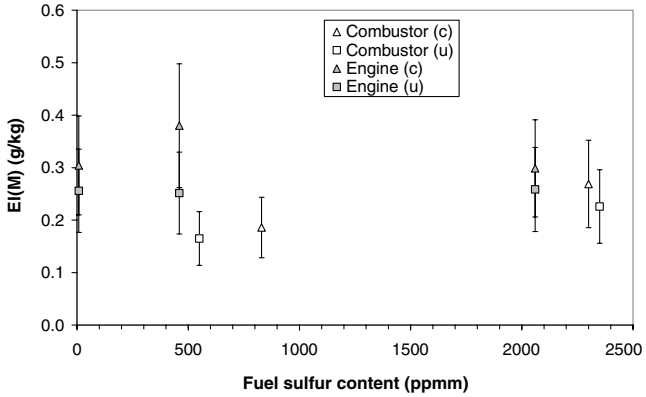

Fig. 3 Mass emission indices $EI(M)$ for different sulfur levels, engine power settings, and probe positions (combustor/engine exit).

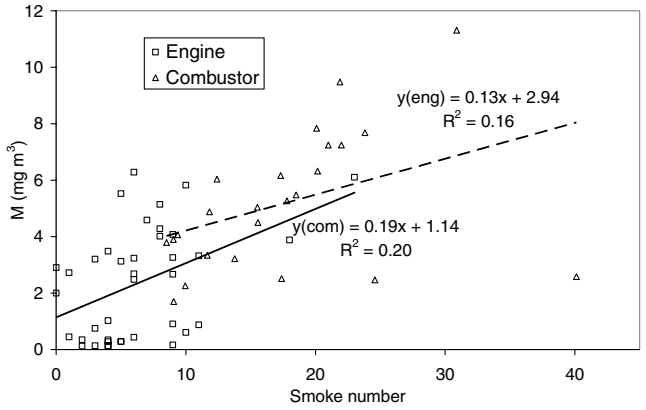

Fig. 4 Correlation of aerosol mass concentration and smoke number for all engine settings and probe positions during the combustor and engine test program.

respectively. Again, $EI(SA)$ and $EI(M)$ show no statistically significant trend, but $EI(N)$ is elevated by a factor of 1.75 for higher sulfur levels. The fact that, on the one hand, $EI(N)$ is reduced for low-sulfur fuel, but $EI(M)$ is not, implies that the mean particle diameter is larger (here ~15%) for the low-sulfur case as seen from Table 6.

Using the data for each individual probe location across the traverse we find poor correlation of the smoke number (SAE) with number concentration ($R^2 = 0.15$), surface area ($R^2 = 0.18$) and mass ($R^2 = 0.20$, slope $= 0.19$ mg/m^3/SAE, intercept$=$ 1.1 mg/m^3), where the latter is depicted in Fig. 4 (squares). Although there was a stronger correlation of smoke number with aerosol mass for the combustor data, there is no correlation of the smoke number with any moment of the aerosol size distribution.

3. Comparison of Combustor and Engine AE Results

There was no significant difference between the aerosol parameters for cruise and uprated cruise for either combustor or engine measurements. Hence, we base the following comparison of combustor and engine aerosol results on the averages over both power settings, where the low-sulfur engine data are excluded, because there are no corresponding data for the combustor. For the medium sulfur case, the ratio of engine and combustor $EI(N)$, $EI(SA)$, and $EI(M)$ was 1.50, 1.74, and 1.80, respectively. We find lower values for the high sulfur case, namely, 1.43, 1.28, and 1.13, respectively. Hence, there is an increase of between 13 to 80% of the EIs through the postcombustor gas path without a trend with respect to fuel sulfur content and moment of the aerosol distribution (N, SA, and M). The observed ratios are close to the expected measurement uncertainties (twice the uncertainty limits) for $EI(N)$, $EI(SA)$, and $EI(M)$, namely, 49, 52, and 62%, respectively. The fact that all ratios are larger than unity, that is, the EIs at the engine exit are larger than at the combustor exit, could be a result of the unaccounted thermophoretic losses during sample extraction. Because the gas temperature at the combustor and engine exit was about 1150 and 600 K, respectively, reduced thermophoretic losses during engine sampling could account for the enhanced EIs at the engine exit. In summary, despite slightly elevated EIs at the engine exit, the mean size and shape of the particle size distribution did not significantly change between combustor and engine exit, that is, there is no evidence for aerosol processing due to, for example, condensation or coagulation. It is noteworthy that for similar operating conditions and no corrections for thermophoretic effects, EI ratios of about 2 with little change to the size and shape of the size distribution have also been reported [17].

D. Modeling Analysis

Model calculations of intraengine trace species chemistry were conducted to match similar conditions achieved during the experiment. Reacting flow modeling of the internal gas path of the engine was based on methods previously developed [2,18–20]. To model the postcombustor evolution of trace chemistry, a computational fluid calculation is used to simulate the nozzle guide vane (NGV) and the rotor of the first high pressure turbine (HPT1) stage. A further 1-D calculation simulates the HPT1 exit to engine nozzle exit. This provides a means for detailed investigations into the potential thermodynamic, fluid mechanic, and chemical kinetic influences on intraengine chemistry. Simulation results suggest an oxidative evolution of NO_y through the postcombustor gas path and reveal a significant impact from temperature and concentration nonuniformities present at the combustor exit and processed through the turbine blade rows.

Reference operational conditions were chosen for the availability of test data and potential for comparative analysis. Because the cruise and uprated cruise power levels in the engine test were similar, two cases differing in fuel sulfur level—high (2060 ppmm) and low (<10 ppmm)—for a single power setting (cruise) were chosen to represent the test conditions. Table 7 provides a summary of the reported post-test simulations.

The flow parameters at combustor exit were based on the results of a thermodynamic cycle model of the engine. Species concentrations were calculated based on chemical equilibrium and adjusted for known measured species concerntrations [2,18–20]. Combustor exit conditions were matched with actual engine measurements along with estimates for species and flow parameters not measured in the tests. Parameters in italics were calculated from engine test data while bold parameters were assumed. Note that the combustion efficiency and the CO EI are consistent. Cases both with and without bypass air dilution of the core flow at the engine exit were investigated. Although simulation of a number of species has been carried out, we restrict our presentation to results for NO_2, HONO, and CO as they can be compared to measurements. Such comparison indicates the modeling methodology can estimate these trace species to within an order of magnitude [10]. Summaries of simulation results are shown in Tables 8 and 9.

Table 7 Summary of simulation conditions

Parameter	Post-test high S	Post-test low S
Combustor exit temperature, K	978–1322	952–1298
Pattern factor (profile shape from data)	30%	30%
Combustor exit pressure, atm	7.7	6.5
Blade surface temperature, K	825	825
Equivalence ratio	*0.152–0.299*	*0.152–0.300*
Combustion efficiency	0.999	0.999
$EINO_x$	6.44	5.58
NO/NO_x	**1.00**	**1.00**
EIS	2.06	0.01
SO_2/SO_x	**1.00**	**1.00**

Table 8 Summary of simulation results for low sulfur

Low sulfur	Combustor exit (IC)	HPT1 NGV exit	HPT1 Rotor exit	Nozzle Exit Air added	Nozzle exit No air	Measured
NO_2, ppbv	——	——	——	534	1080	——
	4.92	170	279	(13.0–1490)	(25.2–2990)	2000 ± 2000
NO_2/NO_y	——	——	——	1.9%	2.1%	——
	0.010%	0.33%	0.54%	(0.065–4.1%)	(0.068–4.5%)	——
HONO, ppbv	——	——	——	540	987	——
	8.30	29.6	62.9	(28.3–1500)	(53.0–2720)	674 ± 140
$HONO/NO_y$	——	——	——	1.9%	1.9%	——
	0.017%	0.058%	0.12%	(0.14–4.2%)	(0.14–4.2%)	2.03 ± 0.5%
CO, ppmv	——	——	——	36.4	67.8	——
	65.4	67.2	68.1	(26.5–45.5)	(49.2–84.0)	30
CO/Co_x	0.33%	0.33%	0.33%	0.33%	0.33%	——

Table 9 Summary of simulation results for high sulfur

High sulfur	Combustor exit (IC)	HPT1 NGV exit	HPT1 Rotor exit	Nozzle exit Air added	Nozzle exit No air	Measured
NO_2, ppbv	——	——		845	1620	——
	7.21	274.0	433	(27.3–2030)	(51.6–3860)	2670 ± 2670
NO_2/NO_y	——	——	——	2.6%	2.7%	——
	0.013%	0.46%	0.73%	(0.12–4.9%)	(0.12–5.1%)	——
HONO, ppbv	——	——	——	780	1310	——
	12.2	37.8	78.4	(46.7–1790)	(85.5–3160)	500 ± 150
$HONO/NO_y$	——	——	——	2.3%)	2.1%	1.12 ± 0.4%
	0.022%	0.064%	0.13%	(0.2–4.3%	(0.2–4.2%)	——
CO, ppmv	——	——	——	36.9	68.0	——
	65.4	67.5	67.5	(26.7–44.7)	(49.1–81.8)	19.2
CO/Co_x	0.33%	0.33%	0.33%	0.32%	0.32%	——

Figure 5 compares NO_2 and HONO evolution through the HPT1 for the high sulfur case. Across the HPT1, production of NO_2 and HONO is significant near and downstream of the turbine blades.

Oxidation of NO to NO_2 and HONO is increased by the higher residence times and lower temperatures of the near blade boundary layer, downstream of the hotter combustor exit temperature exhaust, in particular. Production of NO_2 is also enhanced right above and below the center blade. Increased NO_2 created in freestream locations results from longer residence times in addition to the effect of the circumferential variation in temperature. As the flow speed decreases across the freestream from the suction side of the blade to the pressure side (convex side to concave side), residence time increases. At low and high normalized circumferential distances (near the top and bottom of the HPT1 stage), where the temperatures are lower, increased residence time becomes less important as NO_2 and HONO formation rates fall off significantly, particularly for HONO.

The evolution of NO_2 and HONO across the turbine stage leads to a nonuniform concentration profile at the exit of HPT1. Dispersion of nonuniformities is slow compared to the residence time in the engine, suggesting that they will be present in some form at the engine exit. Note that because of this persistence, in our simulations, nonuniformities present at the end of the HPT1 are maintained through to the exhaust plane in the 1-D stage of the analysis. This results in a spatial range of concentrations that corresponds to as much as 2 orders of magnitude for both HONO and NO_2 and thus a potential uncertainty added to the measurements resulting from probe placement. In contrast, because there is little oxidation activity for CO through the postcombustor flowpath, the range is much smaller (much less than an order of magnitude).

For the low-sulfur case, 1.9–2.0% of NO was oxidized to NO_2 and ~1.9% to HONO through the postcombustor gas path. For the high sulfur case, 2.6–2.7% of NO was oxidized to NO_2 and 2.1–2.3% to HONO. The changes agree in direction and magnitude when compared to the previously described measurements. Axial evolution through the engine shows a relatively larger production of both NO_2 and HONO from the HPT1 exit to nozzle exit relative to that through HPT1 because residence time is much longer, even though oxidation is expected to be less vigorous. For the high sulfur case, where the NO_x EI is higher, the levels of NO_2 through HPT1 are expectedly higher. Creation of NO_2 is delayed across the NGV for the low-sulfur case, likely because of lower NO_x EI of this condition. The sulfur level should not be a factor because SO_2 is oxidized primarily through OH. There could be some interaction between HONO and SO_3 formation, because OH plays an important role in both. However, the simulations show an increase in HONO production with sulfur level that is not detectable in the experimental measurements, apparently following the increased NO_x EI.

Note that the range of nozzle exit results for NO_2 is lower than measurement results because the simulation initial condition (IC) is set with a NO/NO_y ratio of 1.0. As shown in Tables 8 and 9, measured NO_2/NO_y and $HONO/NO_y$ are not 0% at the combustor exit. This difference between simulation and measurement is significant for NO_2. SGA measurements indicate an average NO_2/NO_y ratio of 0.03. This is equivalent to approximately 1500 ppbv of NO_2 and may help explain the difference between measured and calculated NO_2, particularly if the postcombustor oxidation is independent of upstream oxidation [3]. This also suggests that for this engine, the combustor is an important source for NO_2.

IV. Conclusions

A joint U.S./U.K. program was executed to determine the evolution of aerosols and aerosol precursors through the turbine and exhaust nozzle of an aircraft engine typical of the in-service, commercial fleet. Specialist measurement instrumentation was developed for use in separate combustor-only and full-engine tests. A consistent set of data, including CO, NO_x, NO, NO_2, CO_2, O_2, smoke number, carbonaceous aerosol number density and size distribution, SO_2 and HONO, was collected at the exit plane of the combustor. A second probe was used to measure spatially resolved CO, NO_x, NO, NO_2, and CO_2 concentrations. A similar set of data was collected at 460 mm downstream of the exit plane of the engine.

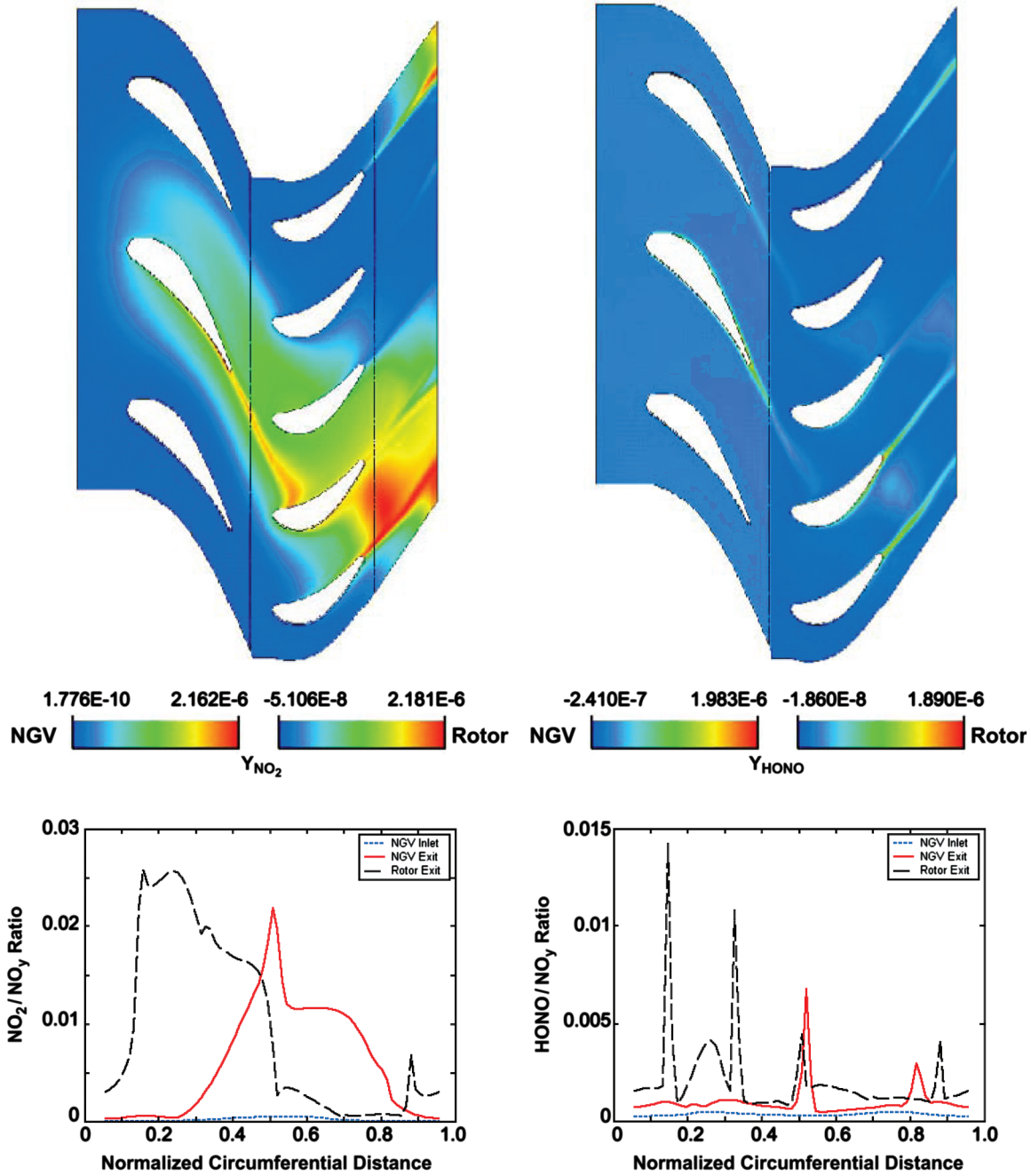

a) NO_2/NO_y profiles **b) $HONO/NO_y$ profiles**

Fig. 5 NO_2 (left) and HONO (right) profiles for high sulfur runs.

The engine was configured to ensure the inlet and outlet conditions for the combustor were similar to those in the combustor test program. In general, combustor AFR and temperature, the parameters that dominate combustion chemistry, matched well, although combustor inlet pressure could not be matched exactly due to engine performance that differed from model predictions. In future studies, it is recommended that such engine tests be performed before the combustor sampling since the combustor is more controllable, providing more accurate matching of operating conditions. Also, if possible, the chosen operating conditions should be more widely separated to enhance any difference in emission values.

The majority of gaseous emissions measured by the SGA did not undergo significant changes through the turbine and were not affected by the sulfur concentration. Measurement of SO_3 in the exhaust is difficult due to losses in the sampling system. An upper limit for detection was obtained, and this limit does no more to constrain the estimate of SO_3 in the exhaust than do the measurements of SO_2 and fuel sulfur content. In future studies of this nature it would be advantageous to develop a measurement technique for SO_3 that is sensitive without being subject to sampling losses, and attempt to monitor other sulfur containing species, specifically H_2SO_4.

Results show no significant dependence of the carbonaceous aerosol parameters on fuel sulfur content and no modifications to the carbonaceous aerosol distribution along the postcombustor gas path. Observations of changes in concentrations of aerosol precursors through the turbine and exhaust nozzle were also obtained. Although it was not possible to determine the conversion of SO_2 to SO_3, oxidation of NO to HONO was measured and compared to model calculations.

Coupled chemical kinetic and flow modeling simulations were also performed to simulate the chemical evolution of aerosol

precursors within the turbine and exhaust nozzle. The models used captured HONO trends correctly and matched the experimental data within the uncertainty of the measurements, which suggests that the modeling approach was valid for the following oxidation chemistry evolution, not only for HONO but also for SO_3.

The oxidation of NO to HONO observed in the present study and its simulation using a kinetic model provides strong support that we understand the chemical kinetics occurring in the postcombustor flowpath. The difficulty in measuring the transient sulfur species SO_3 may be circumvented through a combination of modeling of the sulfur oxidation and measurement of the final oxidative product H_2SO_4. The HONO levels measured in this study indicate that HONO can be a significant NO_y emission, approaching levels often observed for NO_2, and indicate that HONO should be included in any NO_y emissions budget. This study demonstrates that 1) the gaseous emissions that leave the combustor experience an oxidative environment in the engine's turbine and nozzle, 2) the particles generated in the combustor do not change their physical characteristics such as number and size during their transit through the hot section, and 3) little or no correlation can be drawn between smoke number and the physical characteristics of the emission aerosol in either combustor or engine nozzle exhaust.

Acknowledgments

The authors would like to thank QinetiQ [formerly Defense Evaluation and Research Agency (DERA)] and NASA, for providing this unique testing opportunity. This program was funded and executed under a unique Memorandum of Understanding (MoU) between the U.K. and U.S. governments. The U.K. provided, through Department of Trade and Industry (DTI) funding to QinetiQ, specialist test facilities, standard gas analysis, and gas turbine experience. The U.S. provided, through funding from NASA, specialist trace species measurement and gas turbine engine modeling capabilities and experience. In particular, the authors would like to acknowledge the contributions of Chowen Wey (NASA) and Mike Miller (QinetiQ). We further gratefully acknowledge the design and fabrication of the aerosol precursor probe by Robert Howard and Bob Hiers of the U.S. Air Force Arnold Engineering Development Center under NASA sponsorship.

References

[1] Penner, J. E., Lister, D. H., Griggs, D. J., Dokken, D. J., and McFarland, M., "Aviation and the Global Atmosphere," IPCC, Cambridge Univ. Press, Cambridge, U.K., ISBN 0 521 66404 7, 1999.

[2] Lukachko, S. P., Waitz, I. A., Miake-Lye, R. C., Brown, R. C., and Anderson, M. R., "Production of Sulfate Aerosol Precursors in the Turbine and Exhaust Nozzle of an Aircraft Engine," *Journal of Geophysical Research*, Vol. 103, No. D13, 1998, pp. 16159–16174.

[3] Tremmel, H. G., and Schumann, U., "Model Simulations of Fuel Sulphur Conversion Efficiencies in an Aircraft Engine: Dependence on Reaction Rate Constants and Initial Species Mixing Ratios," *Aerospace Science and Technology*, Vol. 3, No. S, 1999, pp. 417–430.

[4] International Standards and Recommended Practices, Environmental Protection, Annex 16, Aircraft Engine Emissions, 2nd ed., International Civil Aviation Organisation (ICAO), July 1993.

[5] SAE Aerospace Recommended Practice, SAE ARP 1256 Rev B, Procedure for the Continuous Sampling and Measurement of Gaseous Emissions from Aircraft Turbine Engines, 1990.

[6] SAE Aerospace Recommended Practice, SAE ARP 1179 Rev C, Aircraft Gas Turbine Engine Exhaust Smoke Measurement, 1997.

[7] SAE Aerospace Recommended Practice, SAE ARP 1533, Procedure for the Calculation of Basic Emission Parameters for Aircraft Turbine Engines, 1996.

[8] McManus, J. B., Nelson, D., Zahniser, M., Mechold, L., Osiac, M., Roepcke, J., and Rousseau, A., "TOBI: A Two-Laser Beam Infrared System for Time-Resolved Plasma Diagnostics of Infrared Active Compounds," *Review of Scientific Instruments*, Vol. 74, No. 5, 2003, pp. 2709–2713.

[9] Berkoff, T. A., Wormhoudt, J., and Miake-Lye, R. C., "Measurement of SO2 and SO3 Using a Tunable Diode Laser System," Environmental Monitoring and Remediation Technologies, *Proceedings of SPIE: The International Society for Optical Engineering*, Vol. 3534, Feb. 1999, pp. 686–693.

[10] "NASA/QinetiQ Collaborative Program—Final Report," NASA CR-2002-211900, Sept. 2002.

[11] Schmid, O., Hagen, D. E., Whitefield, P. D., Trueblood, M. B., Rutter, A. P., and Lilenfeld, H. V., "Methodology for Particulate Characterization in the Exhaust Flows of Gas Turbine Engines," *Aerosol Science and Technology*, Vol. 38, No. 11, 2004, pp. 1108–1122.

[12] Petzold, A., Stein, C., Nyeki, S., Gysel, M., Weingartner, E., Baltensperger, U., Giebel, H., Hitzenberger, R., Döpelheuer, A., Vrchoticky, S., Puxbaum, H., Johnson, M., Hurley, C. D., Marsh, R., and Wilson, C. W., "Properties of Jet Engine Combustion Particles During the PartEmis Experiment: Microphysics and Chemistry," *Geophysical Research Letters*, Vol. 30, No. 13, 2003, p. 1719.

[13] Hitzenberger, R., Giebl, H., Perzold, A., Gysel, M., Nyeki, S., Weingartner, E., Baltensperger, U., and Wilson, C. W., "Properties of Jet Engine Combustion Particles During the PartEmis Experiment: Hygroscopic Growth at Supersaturated Conditions," *Geophysical Research Letters*, Vol. 30, No. 14, 2003, p. 1779.

[14] Wey, C. C. (ed.), "Engine Gaseous, Aerosol Precursor and Particulate Measurements at Simulated Flight Altitude Conditions," NASA TM-1998-208509, ARL-TR-1804, 1998.

[15] Hinds, W. C., *Aerosol Technology*, Wiley, New York, 1999.

[16] Schafer, K., Heland, J., Lister, D. H., Wilson, C. W., Howes, R. J., Falk, R. S., Lindermeir, E., Birk, M., Wagner, G., Haschberger, P., Bernard, M., Legras, O., Wiesen, P., Kurtenbach, R., Brockmann, K. J., Kriesche, V., Hilton, M., Bishop, G., Clarke, R., Workman, J., Caola, M., Geatches, R., Burrows, R., Black, J. D., Herve, P., and Vallly, J., "Nonintrusive Optical Measurements of Aircraft Engine Exhaust Emissions and Comparison with Intrusive Techniques," *Applied Optics*, Vol. 39, No. 3, 2000, pp. 441–455.

[17] Wilson, C. W., Petzold, A., Nyeki, S., Schumann, U., and Zellner, R., "Measurement and Prediction of Emissions of Aerosols and Gaseous Precursors from Gas Turbine Engines (PartEmis): An Overview," *Aerospace Science and Technology*, Vol. 8, No. 2, 2004, pp. 131–143.

[18] Miake-Lye, R. C., Chobot, A. T., Lukachko, S. P., Brown, R. C., Zhang, J., and Waitz, I. A. "Simulation of Post-Combustion Chemical Evolution in Gas Turbine Engines," *Aviation, Aerosols, Contrails, and Cirrus Clouds (A2C3) Workshop*, European Commission Directorate-General for Research, Brussels, July 2000.

[19] Chobot, A. T., "Modeling the Evolution of Trace Species in the Post-Combustor Flow Path of Gas Turbine Engines," M.S. Thesis, Massachusetts Institute of Technology, Cambridge, MA, Sept. 2000.

[20] Brown, R. C., Miake-Lye, R. C., Lukachko, S. P., and Waitz, I. A., "Heterogeneous Reactions in Aircraft Gas Turbine Engines," *Geophysical Research Letters*, Vol. 29, No. 10, 2002, pp. 66-1–66-4.

L. Maurice
Associate Editor